An Algorithm for Correction of Beam Hardening in Computerized X-Ray Tomography

K. K. Mishra, A. M. Quraishi, Shanta Mishra, Ashwani Kumar
Atul Srivastava, K. Muralidhar[1] and P. Munshi

Department of Mechanical Engineering
Indian Institute of Technology, Kanpur – 208 016

ABSTRACT

The paper reports a beam hardening correction algorithm to be applied on the polyenergetic projection data obtained during X-ray tomography of a specimen. Convolution back projection (CBP) algorithm has been used to reconstruct the cross-section of the specimen from the corrected projection data. The beam hardening correction has been applied on simulated test objects and the results have been found to be satisfactory. The number of energy levels taken into account is five for the considered test cases. The algorithm recovers one solution for each energy level. The distribution of errors in each of the solutions depends on the size of the energy level as well as the material density distribution.

Keywords: Beam hardening, X-ray tomography, convolution back projection, flaw detection.

1. INTRODUCTION

The technique of computerized tomography (CT) has established itself as a leading tool in diagnostic radiology over the past three decades and is catching on rapidly in the area of non-invasive measurements (NIM). According to Herman[1], the aim of CT is to obtain information regarding the nature of material occupying exact positions inside the body. CT assigns a number to every point inside the body that corresponds to a specific material property at that point. A suitable physical property for this number is the X-ray or the γ-ray attenuation coefficient of the material. It is obtained from the projection data recorded from an experiment. The reconstruction technique can be the convolution back projection (CBP) algorithm, originally developed by Ramachandran and Laxminarayanan[2], or the algebraic reconstruction technique (ART)[3,4]. In the present study, CBP has been used for the reconstruction of the projection data. It is assumed that the data is available in a parallel beam configuration, Figure 1; this approach has been discussed by Manzoor, *et al*[5]. The filter function used in all the reconstructions of CBP is Hamming 54, a filter that resolves well the smooth variations

[1] Author for correspondence. Manuscript under review.

in the attenuation coefficient and hence the density. For the purpose of displaying the reconstructed image, the CT numbers are read from the CBP output file and appropriate gray levels are assigned to it[6]. Thus by generating a gray scale for each of the projection data, the CT image can be graphically displayed on a grid.

For the correct reconstruction of the object, the input file to the CBP must contain perfect projection values of the object. In the real life experiment, there are many sources of imperfections in the recorded projection data. These include a finite source and detector size, scattering of photons, and polyenergetic photons. The measured projection data must be analytically corrected for all these imperfections before being used for reconstruction. In the present work, corrections for the polyenergetic nature of radiation are discussed.

2. THE PROBLEM OF BEAM HARDENING

Of the many sources of imperfections in the projection data referred above that related to the polyenergetic nature of radiation is called beam hardening. An X-ray source emits photons of multiple energies. A typical energy distribution (spectrum) for an X-ray source (for example, tungsten) has been shown in Figure 2. The coefficient of linear attenuation of the material is usually a function of the incident photon energy. The attenuation at a fixed point is greater for the photons of lower energy. Hence the energy distribution of the X-ray beam changes (hardens) as it passes through the object. This effect is called the hardening of the X-ray beam. The X-ray beams reaching the same point from different directions are likely to have different spectra (having passed through different material before reaching this point) and thus will be attenuated differently at that point. The coefficients of linear attenuation of a given specimen recovered by a tomographic calculation are not the exact values at a given energy. Instead they are a combination of attenuation coefficients emitted at all the energies by the X-ray source. This combination depends upon the type of functional dependence of the attenuation coefficient on the photon energy and the probabilistic energy distribution of the source, i.e. temporal photon statistics. The coefficient of linear attenuation can be mapped to specific properties of the material such as the density distribution. Hence for non-destructive evaluation and non-invasive measurements using computerized tomography (CT) to be reliable, it is necessary to apply corrections for beam hardening. It requires the conversion of polyenergetic

projection data recorded in the experiments into monoenergetic projection data, before reconstruction. In the present study, we have demonstrated beam hardening and its correction by defining computer-generated objects and mathematically calculating the projection data for them. As an example a star shaped object comprising of two materials is presented. For a resolution of 100 rays and 100 views, Figure 3(a) shows the reconstruction without the application of beam hardening correction, and Figure 3(b) is a reconstruction after the application of beam hardening corrections.

3. BEAM HARDENING CORRECTION ALGORITHM

Herman[1] has shown the exact correction for beam hardening in the context of medical imaging when the reconstruction region has only two types of materials. An algorithm for more than two types of materials was also proposed by Herman[7,8]. It was modified by Rama Krishna[9] for applications in NDT. In both cases the monoenergetic reconstruction was carried out at the mean X-ray energy level and a systematic assessment of errors was not attempted. In the present work, we propose an improved algorithm for the correction of beam hardening where (1) the reconstruction can be performed at any of the energies of the incoming radiations (2) the number of material in the object is greater than two, and (3) the iteration scheme can be continued till the errors becomes truly negligible.

The statement of the algorithm is presented first. For a fixed source and detector position in parallel beam geometry (Figure 1), let m denote the monoenergetic ray sum that would have been measured if (1) source was monoenergetic at energy $\bar{e}$, or (2) the material would have been such that its attenuation properties were independent of the incident photon energy. Let p be the polychromatic ray sum that is measured by the detector in the actual experiment that utilizes X-rays. Mathematically m and p are defined in the following manner:

$$m = \int_0^D \mu_{\bar{e}}(z)\, dz \tag{1}$$

$$p = -\ln \int_0^E \tau_e \exp\left[-\int_0^D \mu_e(z)\, dz \right] de \tag{2}$$

Here D is the distance from the source to the detector, $\mu_e(z)$ is the linear attenuation coefficient at energy e at a point on the line from the center of the source to the center of the detector at a distance z from the detector, E is the highest energy level present in the beam, and τ_e is the probability that a detected photon of the X-ray beam (in air between the source and the detector) is at energy e. It is to be recalled that in a complete NDT experiment, m and p represents two-dimensional images with respect to the ray number and the angle of projection. Such images are called sinograms[5].

Beam hardening correction can be done efficiently by performing a polynomial curve fitting between the image data of m and p. In a real experiment we get only the projection data p. Therefore to get a correlation between m and p we have to generate a synthetic data set of m. To approximate the monoenergetic data set m, we need prior (partial) information about the object. Hence as a first guess of the object, we can use the direct reconstruction of the cross-section from the experimental data p using CBP.

Let this approximation be O^0. Collecting a new set of relevant information including the geometry and the size of the object from the reconstructed image, objects X_i can be generated at different selected energies from the X-ray source spectrum. This step requires that the coefficients of linear attenuation at those energies for the particular material be used. The coefficients of linear attenuation for various materials can be obtained from handbooks, or can be obtained experimentally in a calibration experiment by using a single line of the X-ray beam at a time. From the generated objects X_i, the approximate projection data $\overline{m}_i$'s can be obtained from Equation (3). Even for a defect free sample $\overline{m}_i$ is different from m_i due to the discretization of the reconstruction region. But if defects are present in the sample, then m_i will have information about these defects. This important information will not be present $\overline{m}_i$ in the first iteration.

The next step is to generate an artificial polyenergetic data $\bar{p}$ using Equation (4) with $\tau(j)$ as the probability that a detected photon of the X-ray beam is at energy $e(j)$. This is needed in order to get a correlation between $\bar{m}_i$ and $\bar{p}$. The correlation function (f_i) can be applied to the actual measured data p recorded in the experiment. Theoretically, p and $\bar{p}$ should be identical. But the experimental data p varies from $\bar{p}$ calculated, because of reasons such that consideration of discrete and finite number of energies while calculating $\bar{p}$ and experimental errors involved. The major source of the difference is defects that are likely to be present in the sample being tested. Identifying these defects is the goal of the present work. The approximate projection data $\bar{m}$ and $\bar{p}$ can be determined as follows:

$$\bar{m} = \sum_{i=1}^{I} \mu_e^i \, z^i \tag{3}$$

$$\bar{p} = - \ln \sum_{j=1}^{J} \tau_{e(j)} \exp\left[- \sum_{i=1}^{I} \mu_{e(j)}^i \, z^i \right] \tag{4}$$

From the above discussion, it is clear that $\bar{m}_i$ approximates m_i and $\bar{p}$ approximates p. Central to the proposed numerical algorithm is the observation that the function $f_i(\bar{p})$ defined as:

$$\bar{m}_i \approx f_i(\bar{p}) \tag{5}$$

approximates $f_i(p)$, namely

$$m_i \approx f_i(p) \tag{6}$$

In words, the correlation function f determined from the approximate projection data (mono and polyenergetic) is sensibly close to the exact function. Further, it can be iteratively improved.

To get this correlation function f_i a curve fitting strategy between $\bar{m}_i$ and $\bar{p}$ has been utilized. The most inexpensive curve-fitting route is to adopt a polynomial function for f, and determine its coefficients, for example, by the least squares

technique. Any other image processing operation such as correlation and image registration can also be employed. The corrections obtained and the number of iterations required in each case will however be different. This function f_i obtained after correlation can then be applied on the experimental data p to obtain the equivalent monoenergetic projection data set m_i of the object under test as in Equation (6). CT algorithms such as CBP can be applied to m_i.

The numerical algorithm can now be summarized as follows: The unknown object cross-section is first assessed using polyenergetic data. The function f_i is estimated with respect to this object. The first iterate of the correlation function is applied to the experimentally recorded polyenergetic data of the test object. The first reconstruction O^{i1} is carried out using CBP from $f_i(p)$ as it approximates m_i. This completes the first iteration of beam hardening correction. Using the individual monoenergetic data sets, the cross-section can be repeatedly reconstructed (using, say CBP). The next step is to compare with the initial guess O^0. If new features are visible, for example a crack or the set of dislocations, the initial guess is improved accordingly and all the steps are repeated again. If new features are not visible then the correction algorithm will stop. The solutions obtained at different energies can now be displayed. The numerical algorithm described here is summarized in the flow chart of Figure 4.

4. RESULTS AND DISCUSSION

The beam hardening correction algorithm has been tested for computer generated objects and has been found to yield good results. A few of the test cases considered are presented here. The numerical values of peaks in the X-ray source spectrum used in the simulation are given in Table 1. Five different energies have been considered; the reconstruction region is assumed to carry three different types of materials. Symbols $\mu^a_{e(j)}$, $\mu^b_{e(j)}$ and $\mu^c_{e(j)}$ are the coefficients of linear attenuation for the three types of materials namely *'a'*, *'b'* and *'c'* respectively at energy $e_{(j)}$.

Symbols used in all the reconstructed figures and simulated objects have the following meaning:

Min: Minimum value of the gray scale for material density

Max: Maximum value of the gray scale for material density

LAvg: Average value of the gray levels on the horizontal centerline

AAvg: Cross-sectionally averaged value of the gray level.

Case 1: The object considered is a circle made up of material '*a*' with three circular holes, one filled with material '*b*' and two filled with material '*c*'. The number of rays and the number of views used in calculating projection data are 128 × 128 respectively. Figures 4, 5 and 6 shows the images obtained after applying beam hardening correction to the experimental data of the object, at energies $e_{(1)}\,(\tau_{e(1)} = 0.1)$, $e_{(2)}\,(\tau_{e(2)} = 0.3)$ and $e_{(4)}\,(\tau_{e(4)} = 0.2)$ respectively. These figures can be compared to understand the effect of change in probability $\tau_{e(j)}$ on the monoenergetic reconstruction of the object after the beam-hardening correction on the projection data at that energy. All energies with different probabilities have been considered. Figure 5(a) is the simulated object at energy $e_{(1)}$. Figure 5(b) is the reconstruction of the experimental data by directly applying CBP to it. Figure 5(c) is the reconstruction of the experimental data after applying beam hardening correction to it at energy $e_{(1)}$. Figure 6, at energy $e_{(2)}$ and Figure 7, at $e_{(4)}$ have the same reconstruction procedure as given for Figure 5. Here we have considered a defect free sample and hence we do not get any new features visible after first iteration of the algorithm. Hence beam-hardening correction is complete after the first iteration, and its reconstruction has been shown. From these images it is clear that beam hardening correction will be more effective for those energies which have higher probabilities $\tau_{e(j)}$. As the probability of detected photon is the least at energy $e_{(1)}$, the experimental data has least contribution from the photons of this energy. This can also be observed from Equation (4). Hence, the experimental data does not contain much information about the coefficient of linear attenuation of the materials in the object at energy $e_{(1)}$. This explains the non-uniform reconstruction at this energy, as shown in the Figure 5(c). It can be observed from the figure that the reconstruction after applying beam hardening correction at energy $e_{(2)}$ (which has highest probability) is more uniform than monoenergetic reconstruction at energy $e_{(1)}$ and $e_{(4)}$. In principle the algorithm works for all the energies. It is recommended that beam-

hardening correction at the energy with the highest probability $\tau_{e(j)}$ be used in measurements related to NDT.

Case 2: The object considered is circular in cross-section made up of material '*a*' with a star shaped hole inside, filled with material '*b*'. The material '*b*' has a crack in it. The small holes are filled with material '*c*'. Results with beam hardening correction for this object at all the five energies has been presented in Figures 8-12. As the energy $e_{(3)}$ has highest probability $\tau_{e(j)}$ in the X-ray spectrum, the working of the algorithm is explained here taking beam-hardening correction at energy $e_{(3)}$ as an example, Figure 10. The reconstruction of the experimental data (p) obtained after the X-ray tomography of the object is shown in Figure 10(a). From this reconstruction the object type (O^0) can be identified. Crack is not an intrinsic property of the object; it is present in the particular sample of the object which is defective. The object O^0 is simulated at all five energies called X_i. X_3 is shown in Figure 10(b). Monoenergetic ($\overline{m}_i$) and polychromatic ($\overline{p}$) projection data is calculated from X_i's as explained above using Equations (3) and (4) respectively. In the present discussion, the number of rays per view are 256 and number of views are 256. Now, the function f_i, which correlates $\overline{p}$ and $\overline{m}_i$ can be found out. Here least square curve fitting[10] has been used to get the coefficients of the polynomial function f_i of degree three. This function is of the form:

$$\overline{m}_3 = a_0 + a_1\ \overline{p} + a_2\ \overline{p}^2 + a_3\ \overline{p}^3 \qquad (7)$$

The coefficients for curve fitting between $\overline{p}$ and $\overline{m}_3$ are given in Table 2. The coefficients a_0, a_1, a_2 and a_3 are used to find m_i's, the monoenergetic data set for each energy. CBP is applied to the data for all the five energies. The first monoenergetic reconstruction at energy $e_{(3)}$ is shown in Figure 10(c). In the figure a crack is clearly visible. It is a new feature as it was not present in the initial guess O^0 of the object. It is clear that the beam hardening correction should now be continued. In the second iteration, the guessed object O^1 is the one obtained from the previous iteration. This is a star-shaped object with a crack at the location where it appeared in

previous monoenergetic reconstruction, Figure 10(d). The entire correction process is repeated with O^1. The monoenergetic reconstruction after the second iteration is shown in Figure 10(e). The coefficients of curve fitting for second iteration are given in Table 2. We do not observe any new features in the reconstruction after second iteration; hence the beam-hardening correction algorithm can be stopped at this stage.

Case 3: Here the object is identical to case 2 with equal number of rays and views, but the degree of polynomial curve fitting is increased to four instead of three. The correction procedure is identical to that in Case 2. The coefficients of the curve fitting at energy $e_{(3)}$ are given in Table 3. The results for this geometry are shown in Figures 13-17. Comparing the results of case 2 and case 3, it can be readily inferred that the beam hardening correction procedure leads to an improvement in the monoenergetic reconstruction. The improvement in the reconstruction however requires more computational power and time. In the present discussion, we have taken with 256 views and 256 rays. As this number is increased to 512 and later to 1024, the computational time rapidly increases. Hence, for general application the third degree polynomial curve fit is good enough for beam hardening correction. It can be increased in principle for higher accuracy.

5. CONCLUSIONS

Correction for beam hardening is necessary in computerized tomography when the radiation source is polyenergetic. An algorithm that can be used for this correction has been proposed. The test objects considered consisted of three materials but the algorithm could be used with objects that contain more than three materials as well. For the correction of beam hardening, the spectrum of the X-ray source and the coefficients of linear attenuation of the materials in the object at these energies are required. This makes the computer code for beam hardening correction specific to the radiation source and the test materials.

Beam hardening correction can be done at any of the lines of the X-ray spectrum. Results obtained in the present work show that the mean energy (which has the highest probability of detection) is adequate. While any correlation techniques can also be used in the algorithm, polynomial curve fitting was seen to be the least expensive, and the results obtained were good enough for general applications. The degree of polynomial

need not be more than three for a good monoenergetic reconstruction. Thus the proposed algorithm was found to be quite robust.

ACKNOWLEDGEMENTS

The work reported in this paper was possible due to financial support of DRDL, Hyderabad. Useful discussions with Dr S. Vathsal, Dr C. Muralidhar, Shri G. V. Siva Rao and Shri S. Chakraborthy is gratefully acknowledged.

REFERENCES

1. Herman G. T. (1980): *Image reconstruction from projections: The fundamentals of computerized tomography*, Academic Press, New York.
2. Ramachandran G. N. and Lakshminaryanan A. V. (1970): *Three- dimensional reconstruction from radiographs and electron micrographs: Application of convolution instead of Fourier transforms.* Proc. Natl. Acad., USA, **68**: 2236-240.
3. Singh Suneet, Muralidhar K. and Munshi P. (2002): *Image reconstruction from incomplete-projection data using combined ART_CBP algorithm*, Defence Science Journal, **52 (3)**: 303-316.
4. Natterer F. (1986): *The Mathematics of the Computerized Tomography*, John Wiley & Sons, New York.
5. Manzoor M. F., Yadav P., Muralidhar K. and Munshi P. (2001): *Image reconstruction of simulated specimens using convolution back projection*, Defence Science Journal, **51(2)**: 175-187.
6. *Development of software for image reconstruction and error analysis for Computerized Tomography*, DRDL Progress Report (Phase I), December 1999.
7. Herman G.T. (1979): *Correction for Beam Hardening in Computed Tomography*, Phys. Med. Boil. 24: 81-106.
8. Herman G. T. (1979): *Demonstration of Beam Hardening Correction in Computed Tomography of the Head*, J. Computed Assist. Tomography, **3**: 373-378.
9. Rama Krishna K. (2000): *Simulation and Correction of the Beam Hardening effect in X-ray Tomography*, M. Tech Thesis, IIT Kanpur.
10. Jain M.K., Jain R.K. and Iyengar S.R.K. (1999): Numerical methods for Scientific and Engineering Computation, New Age International [P] Ltd., 3rd Edition.

Table 1: Spectrum of the X-ray source

j	$\tau_{e(j)}$	$\mu^{a}_{e(j)}$ **(cm^{-1})**	$\mu^{b}_{e(j)}$ **(cm^{-1})**	$\mu^{c}_{e(j)}$ **(cm^{-1})**	**Energy (k eV)**
1	0.1	0.265	0.999	0.632	41
2	0.3	0.226	0.595	0.411	52
3	0.3	0.210	0.416	0.313	60
4	0.2	0.183	0.265	0.224	84
5	0.1	0.174	0.208	0.191	100

Table 2: Coefficients of curve fitting (using cubic polynomial) for star shaped object at energy $\boldsymbol{e_3}$.

Coefficients of Polynomial	**Iterations**	
	1^{st}	2^{nd}
a_0	-0.006708	-0.006618
a_1	1.095818	1.094304
a_2	-0.332331	-0.326000
a_3	0.183701	0.176194

Table 3: Coefficients of curve fitting (using fourth order polynomial) for star shaped object at energy $\boldsymbol{e_3}$.

Coefficients of Polynomial	**Iterations**	
	1^{st}	**2^{nd}**
a_0	0.001211	0.001371
a_1	0.940517	0.936821
a_2	0.503585	0.525740
a_3	-1.491593	-1.539218
a_4	1.120672	1.153372

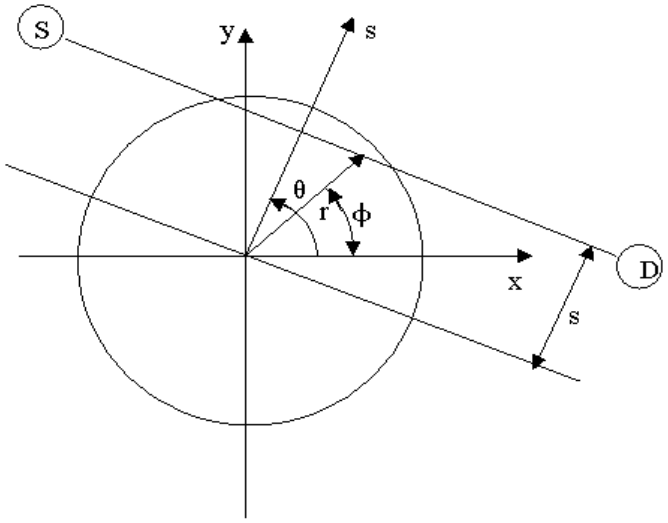

Figure 1: Parallel beam geometry for the collection of projection data

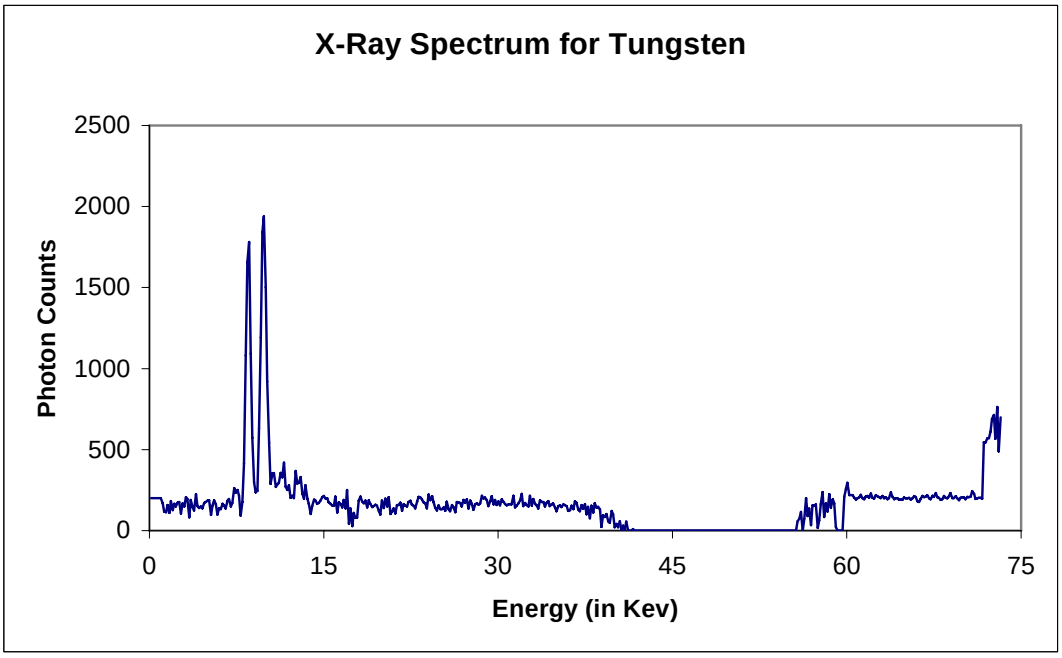

Figure 2: A typical X-ray energy spectrum for tungsten.

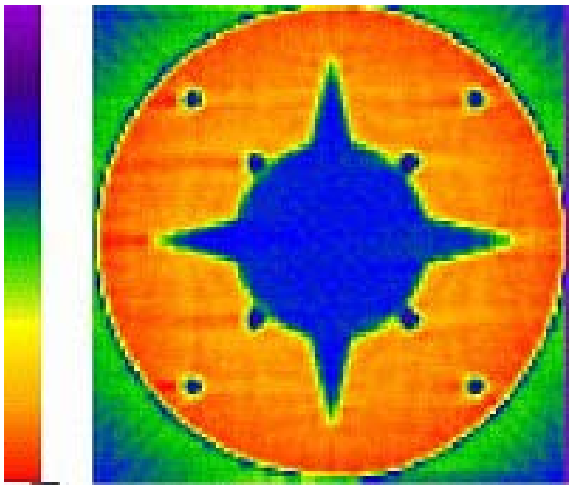

Min = 0.0925 Max = 0.6775
LAvg = 0.3397 AAvg = 0.4922

(a)

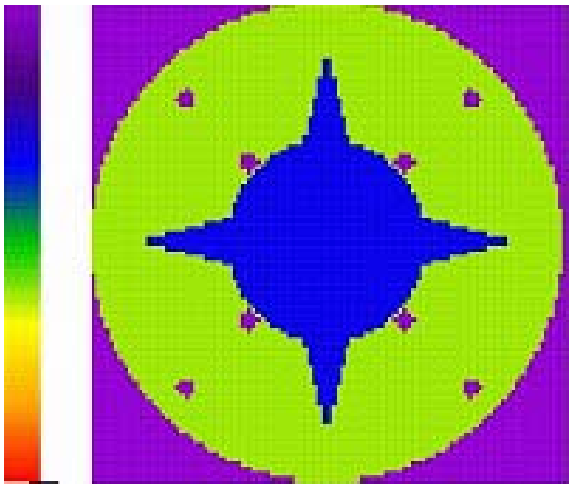

Min = 0.0000 Max = 0.4160
LAvg = 0.2594 AAvg = 0.3531

(b)

Figure 3: Reconstructed star shaped object of a two-density material: (a) without the application of beam hardening correction (b) after the application of beam hardening corrections. Note that in (b), the small circles are well-resolved.

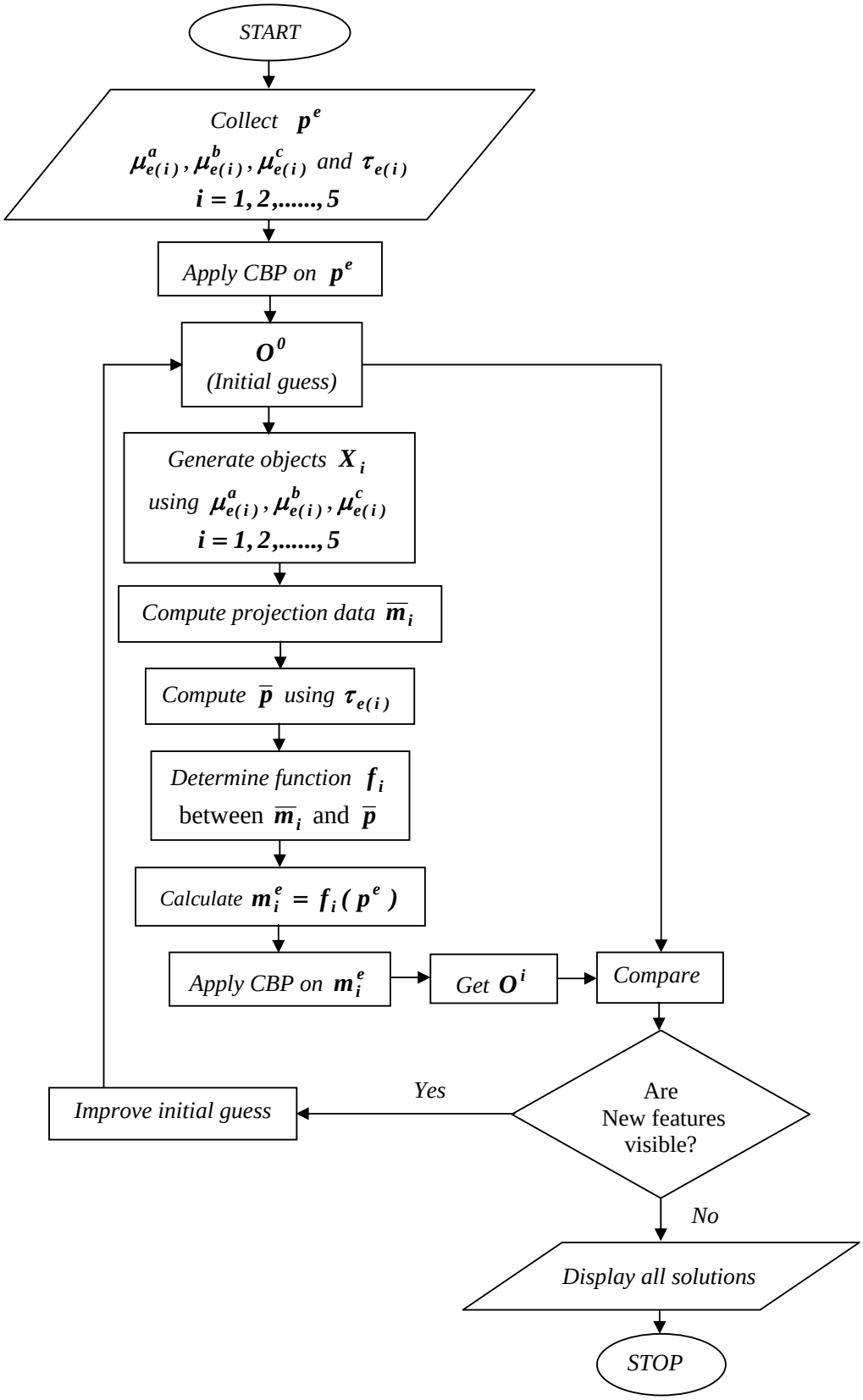

Figure 4: Flow chart for the beam hardening correction procedure.

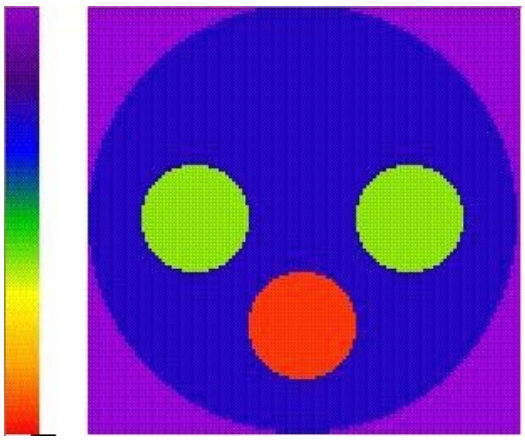

Min = 0.0000 Max = 0.9990
LAvg = 0.4485 AAvg = 0.3793

(a)

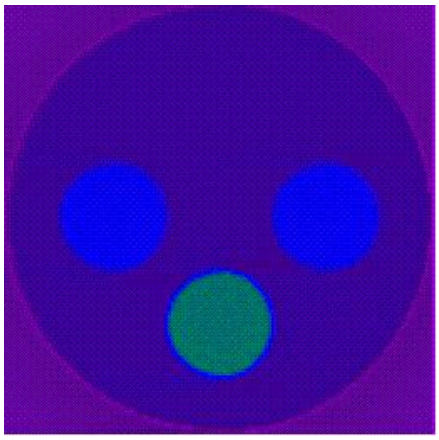

Min = 0.0555 Max = 0.4675
LAvg = 0.2711 AAvg = 0.2499

(b)

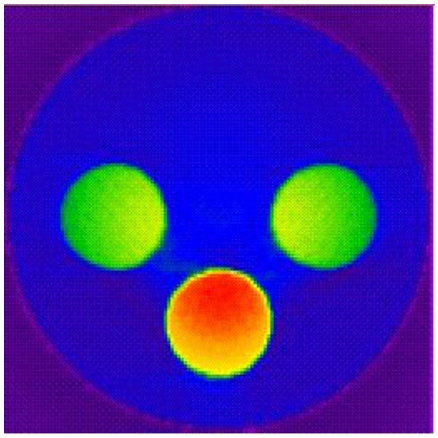

Min = 0.0432 Max = 1.0478
LAvg = 0.4575 AAvg = 0.3788

(c)

Figure 5: Correction for beam hardening on simulated data with 128 rays and 128 views: (a) Simulated object at energy $\boldsymbol{e_1}$, (b) Reconstruction of the generated experimental data by directly applying CBP, (c) Reconstruction of the corrected data at energy $\boldsymbol{e_1}$.

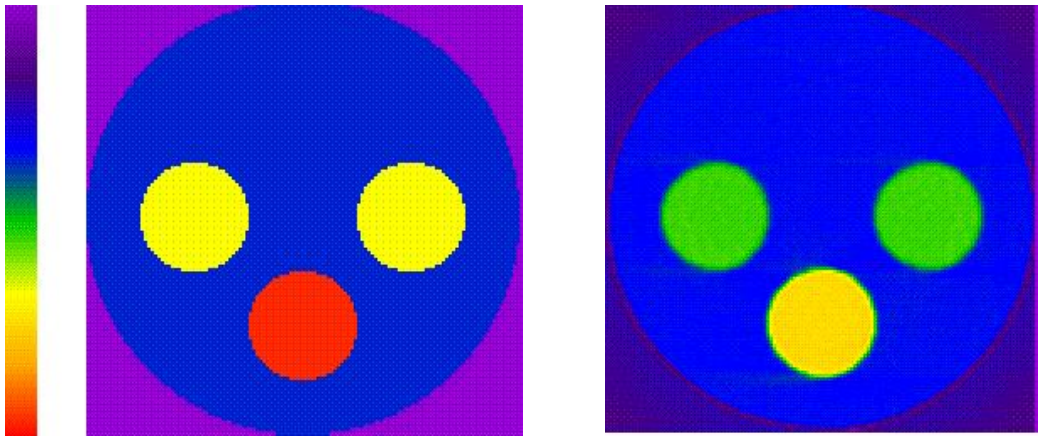

Min = 0.0000 Max = 0.5950
LAvg = 0.3185 AAvg = 0.2835

(a)

Min = 0.0555 Max = 0.4675
LAvg = 0.2711 AAvg = 0.2499

(b)

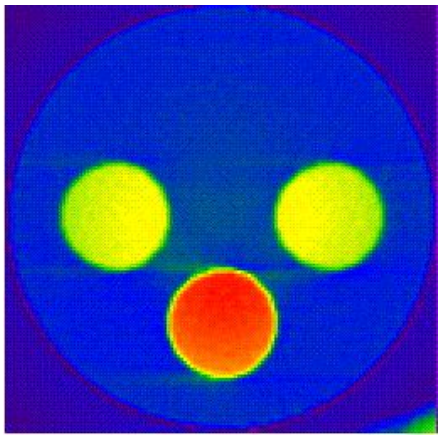

Min = 0.0523 Max = 0.6127
LAvg = 0.3197 AAvg = 0.2837

(c)

Figure 6: Correction for beam hardening on simulated data with 128 rays and 128 views: (a) Simulated object at energy e_2, (b) Reconstruction of the generated experimental data by directly applying CBP, (c) Reconstruction of the corrected data at energy e_2.

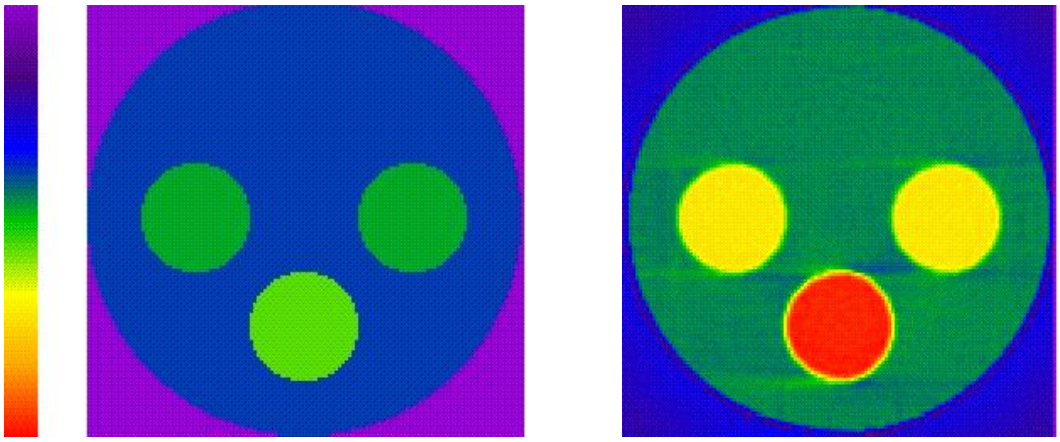

Min = 0.0000 Max = 0.2650
LAvg = 0.2035 AAvg = 0.1958

(a)

Min = 0.0555 Max = 0.4675
LAvg = 0.2711 AAvg = 0.2499

(b)

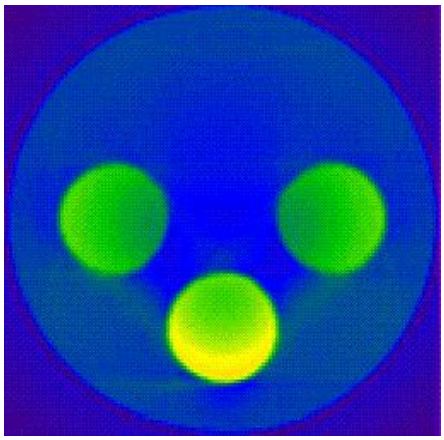

Min = 0.0537 Max = 0.3434
LAvg = 0.1992 AAvg = 0.1964

(c)

Figure 7: Correction for beam hardening on simulated data with 128 rays and 128 views: (a) Simulated object at energy e_4, (b) Reconstruction of the generated experimental data by directly applying CBP, (c) Reconstruction of the corrected data at energy e_4.

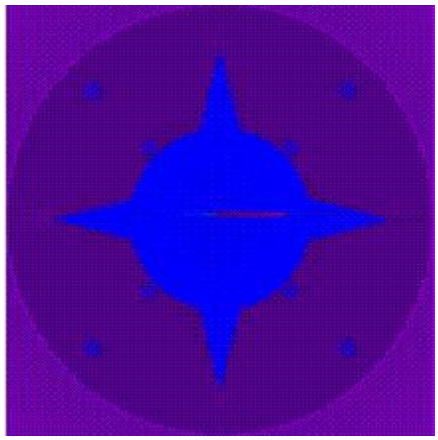

Min = 0.0536 Max = 0.5455
LAvg = 0.3891 AAvg = 0.2812

(a)

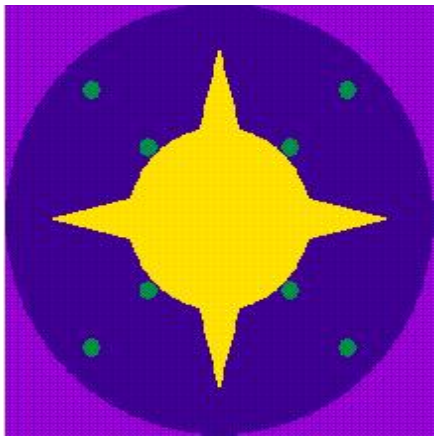

Min = 0.0000 Max = 0.9990
LAvg = 0.8384 AAvg = 0.4750

(b)

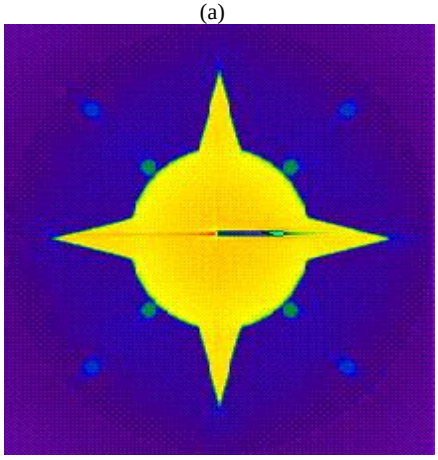

Min = - 0.2284 Max = 1.3594
LAvg = 0.8455 AAvg = 0.4763

(c)

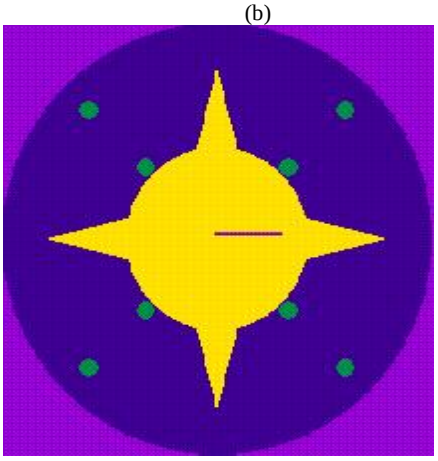

Min = 0.0000 Max = 0.9990
LAvg = 0.8384 AAvg = 0.4731

(d)

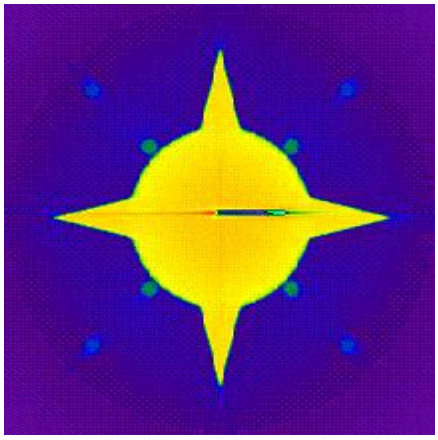

Min = -0.2370 Max = 1.3680
LAvg = 0.8501 AAvg = 0.4770

(e)

Figure 8: Correction for beam hardening on simulated data for star shaped object with a crack for 256 rays and 256 views: (a) Reconstruction of the generated experimental data by directly applying CBP, (b) Simulated object without the crack at energy e_1, (c) Reconstruction after the first iteration of beam hardening correction using cubic polynomial at energy e_1, (d) Simulated object with the crack at energy e_1, (e) Reconstruction after the second iteration of beam hardening correction using cubic polynomial at energy e_1.

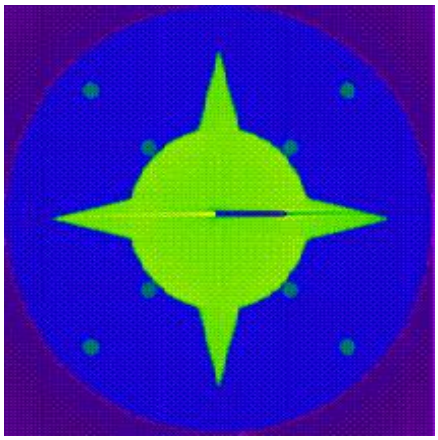

Min = 0.0536 Max = 0.5455
LAvg = 0.3891 AAvg = 0.2812

(a)

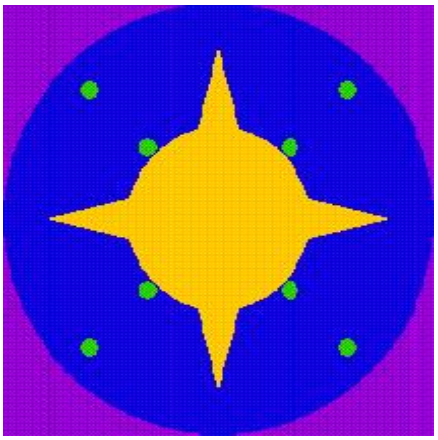

Min = 0.0000 Max = 0.5950
LAvg = 0.5143 AAvg = 0.3314

(b)

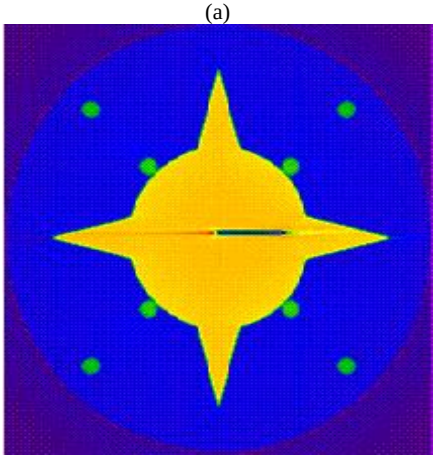

Min = -0.0147 Max = 0.7655
LAvg = 0.5129 AAvg = 0.3325

(c)

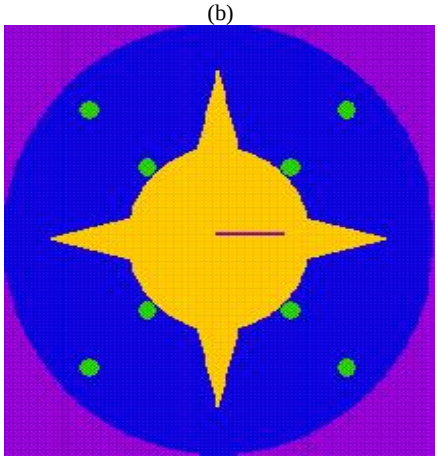

Min = 0.0000 Max = 0.5950
LAvg = 0.5143 AAvg = 0.3303

(d)

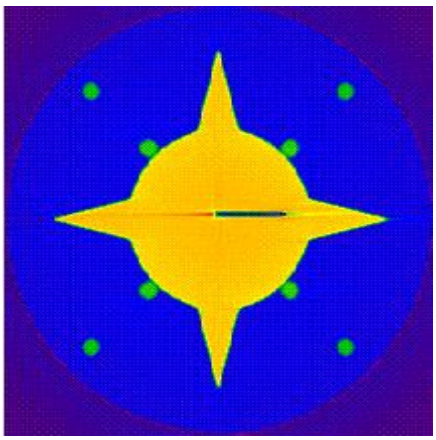

Min = -0.0169 Max = 0.7677
LAvg = 0.5140 AAvg = 0.3327

(e)

Figure 9: Correction for beam hardening on simulated data for star shaped object with a crack for 256 rays and 256 views: (a) Reconstruction of the generated experimental data by directly applying CBP, (b) Simulated object without the crack at energy e_2, (c) Reconstruction after the first iteration of beam hardening correction using cubic polynomial at energy e_2, (d) Simulated object with the crack at energy e_2, (e) Reconstruction after the second iteration of beam hardening correction using cubic polynomial at energy e_2.

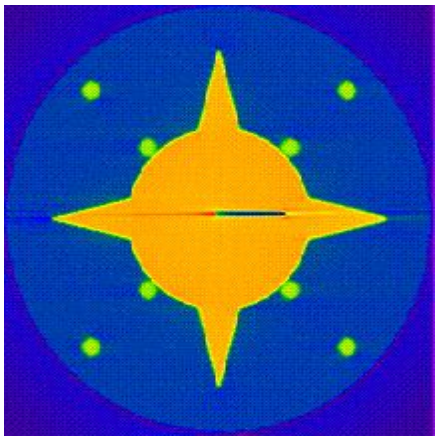

Min = 0.0536 Max = 0.5455
LAvg = 0.3891 AAvg = 0.2812

(a)

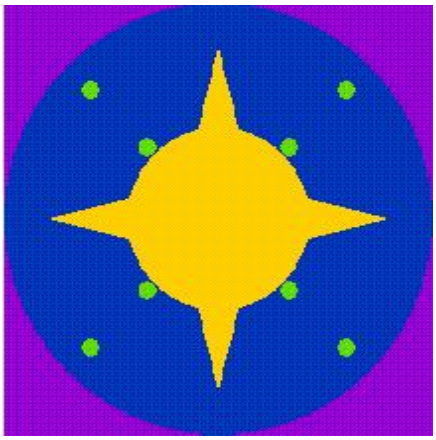

Min = 0.0000 Max = 0.4160
LAvg = 0.3709 AAvg = 0.2689

(b)

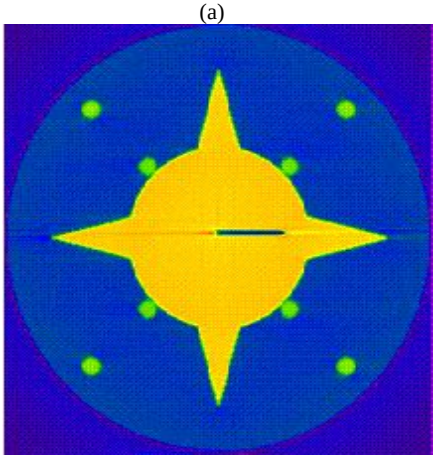

Min = 0.0399 Max = 0.5015
LAvg = 0.3656 AAvg = 0.2697

(c)

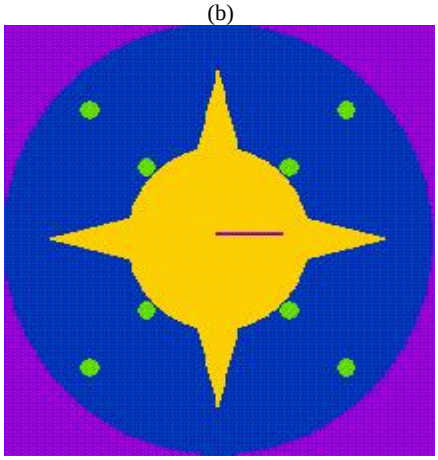

Min = 0.0000 Max = 0.4160
LAvg = 0.3709 AAvg = 0.2681

(d)

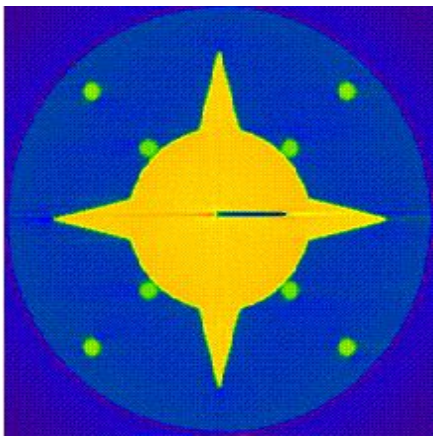

Min = 0.0401 Max = 0.5009
LAvg = 0.3653 AAvg = 0.2697

(e)

Figure 10: Correction for beam hardening on simulated data for star shaped object with a crack for 256 rays and 256 views: (a) Reconstruction of the generated experimental data by directly applying CBP, (b) Simulated object without the crack at energy e_3, (c) Reconstruction after the first iteration of beam hardening correction using cubic polynomial at energy e_3, (d) Simulated object with the crack at energy e_3, (e) Reconstruction after the second iteration of beam hardening correction using cubic polynomial at energy e_3.

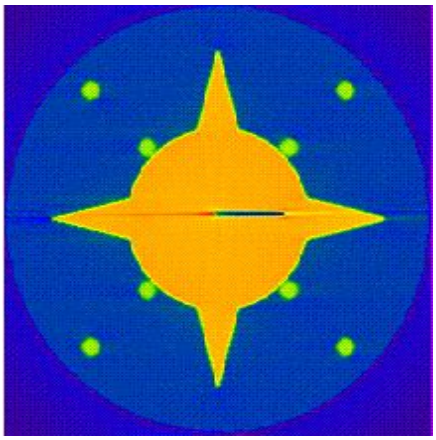

Min = 0.0536 Max = 0.5455
LAvg = 0.3891 AAvg = 0.2812

(a)

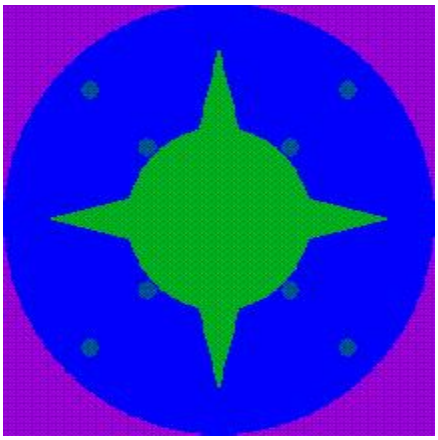

Min = 0.0000 Max = 0.2650
LAvg = 0.2471 AAvg = 0.2065

(b)

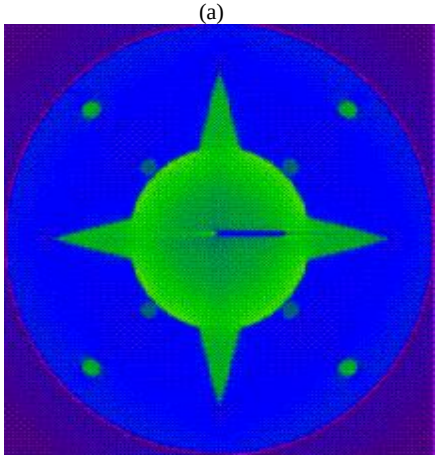

Min = 0.0144 Max = 0.3035
LAvg = 0.2396 AAvg = 0.2071

(c)

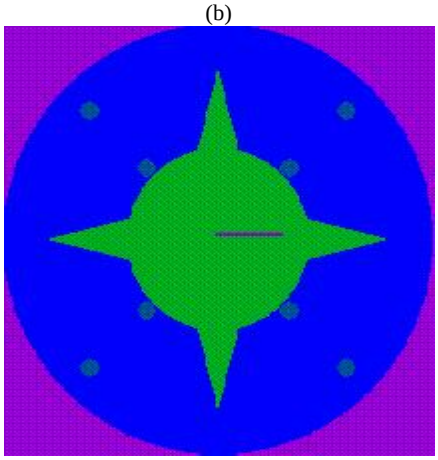

Min = 0.0000 Max = 0.2650
LAvg = 0.2471 AAvg = 0.2060

(d)

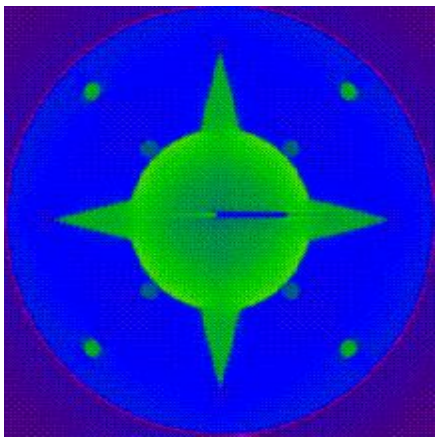

Min = 0.0149 Max = 0.3033
LAvg = 0.2383 AAvg = 0.2069

(e)

Figure 11: Correction for beam hardening on simulated data for star shaped object with a crack for 256 rays and 256 views: (a) Reconstruction of the generated experimental data by directly applying CBP, (b) Simulated object without the crack at energy e_4, (c) Reconstruction after the first iteration of beam hardening correction using cubic polynomial at energy e_4, (d) Simulated object with the crack at energy e_4, (e) Reconstruction after the second iteration of beam hardening correction using cubic polynomial at energy e_4.

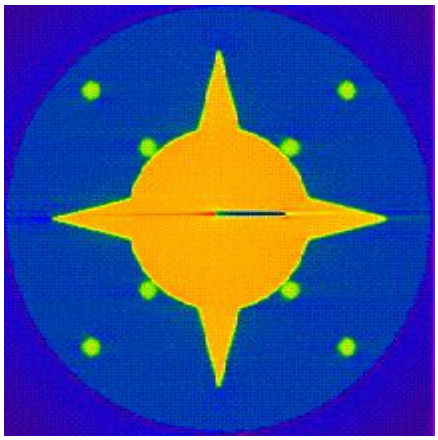

Min = 0.0536 Max = 0.5455
LAvg = 0.3891 AAvg = 0.2812

(a)

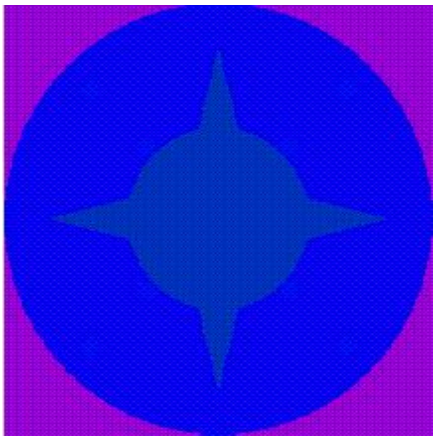

Min = 0.0000 Max = 0.2080
LAvg = 0.2006 AAvg = 0.1837

(b)

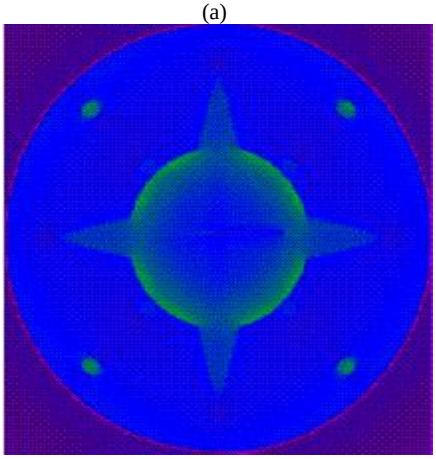

Min = 0.0045 Max = 0.2564
LAvg = 0.1922 AAvg = 0.1843

(c)

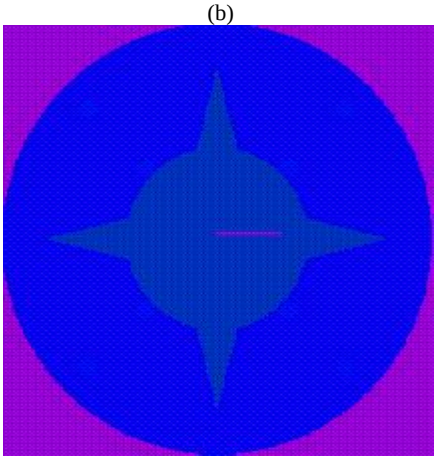

Min = 0.0000 Max = 0.2080
LAvg = 0.2006 AAvg = 0.1833

(d)

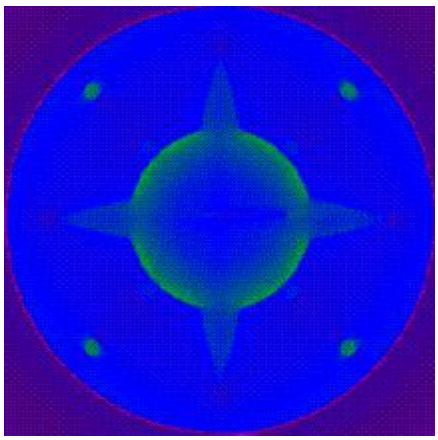

Min = 0.0056 Max = 0.2562
LAvg = 0.1896 AAvg = 0.1839

(e)

Figure 12: Correction for beam hardening on simulated data for star shaped object with a crack for 256 rays and 256 views: (a) Reconstruction of the generated experimental data by directly applying CBP, (b) Simulated object without the crack at energy e_5, (c) Reconstruction after the first iteration of beam hardening correction using cubic polynomial at energy e_5, (d) Simulated object with the crack at energy e_5, (e) Reconstruction after the second iteration of beam hardening correction using cubic polynomial at energy e_5.

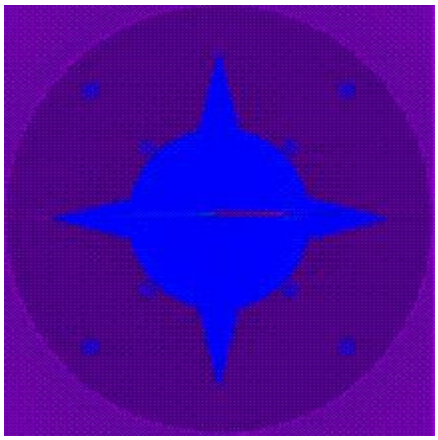

Min = 0.0536 Max = 0.5455
LAvg = 0.3891 AAvg = 0.2812

(a)

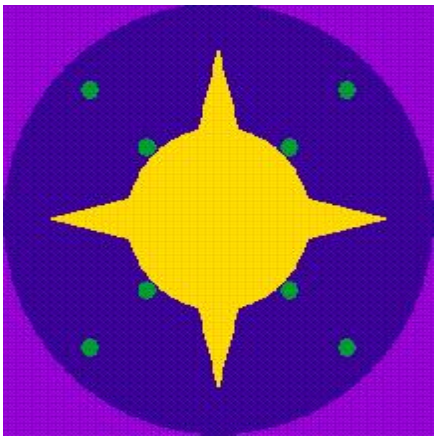

Min = 0.0000 Max = 0.9990
LAvg = 0.8384 AAvg = 0.4750

(b)

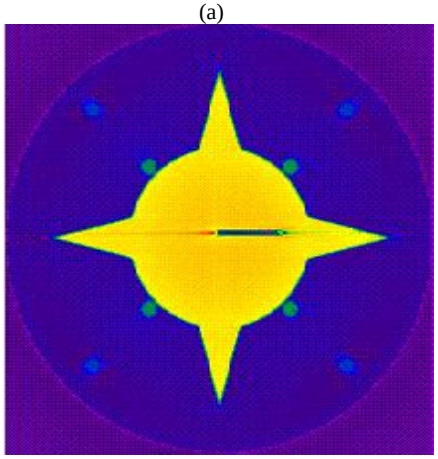

Min = -0.1191 Max = 1.3355
LAvg = 0.8079 AAvg = 0.4742

(c)

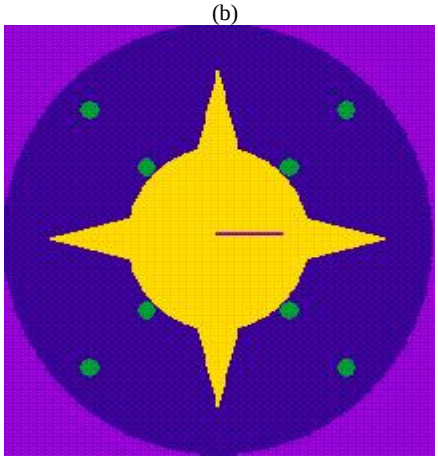

Min = 0.0000 Max = 0.9990
LAvg = 0.8384 AAvg = 0.4731

(d)

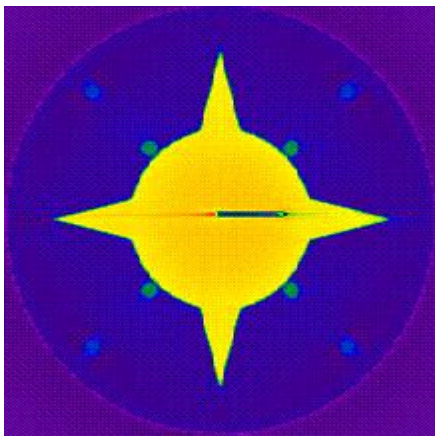

Min = -0.2370 Max = 1.3680
LAvg = 0.8501 AAvg = 0.4770

(e)

Figure 13: Correction for beam hardening on simulated data for star shaped object with a crack for 256 rays and 256 views: (a) Reconstruction of the generated experimental data by directly applying CBP, (b) Simulated object without the crack at energy e_1, (c) Reconstruction after the first iteration of beam hardening correction using fourth degree polynomial at energy e_1, (d) Simulated object with the crack at energy e_1, (e) Reconstruction after the second iteration of beam hardening correction using fourth degree polynomial at energy e_1.

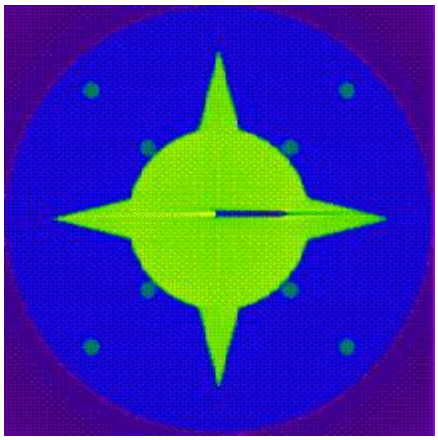

Min = 0.0536 Max = 0.5455
LAvg = 0.3891 AAvg = 0.2812

(a)

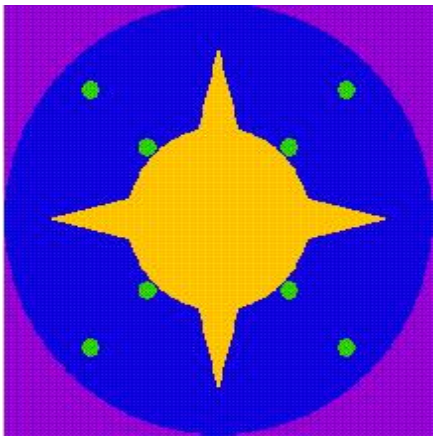

Min = 0.0000 Max = 0.5950
LAvg = 0.5143 AAvg = 0.3314

(b)

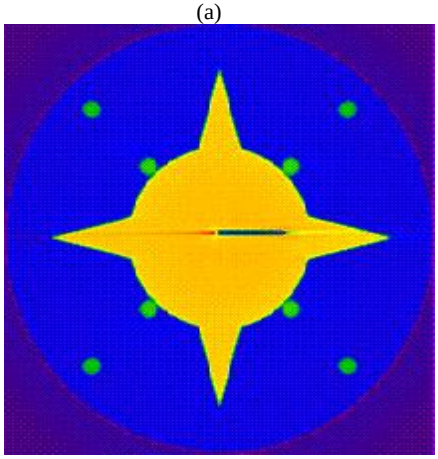

Min = 0.0084 Max = 0.7604
LAvg = 0.5049 AAvg = 0.3321

(c)

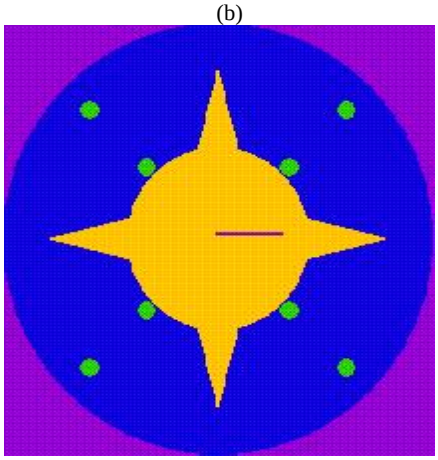

Min = 0.0000 Max = 0.5950
LAvg = 0.5143 AAvg = 0.3303

(d)

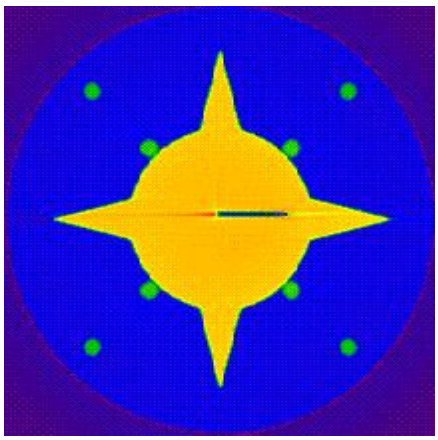

Min = -0.0169 Max = 0.7677
LAvg = 0.5140 AAvg = 0.3327

(e)

Figure 14: Correction for beam hardening on simulated data for star shaped object with a crack for 256 rays and 256 views: (a) Reconstruction of the generated experimental data by directly applying CBP, (b) Simulated object without the crack at energy e_2, (c) Reconstruction after the first iteration of beam hardening correction using fourth degree polynomial at energy e_2, (d) Simulated object with the crack at energy e_2, (e) Reconstruction after the second iteration of beam hardening correction using fourth degree polynomial at energy e_2.

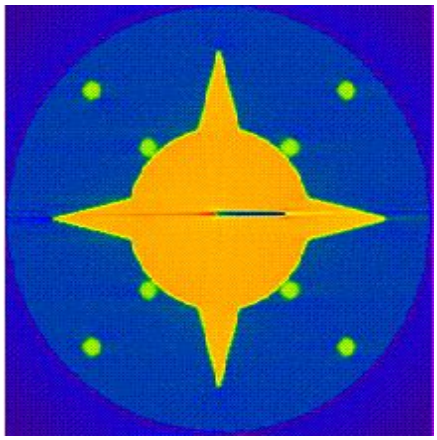

Min = 0.0536 Max = 0.5455
LAvg = 0.3891 AAvg = 0.2812

(a)

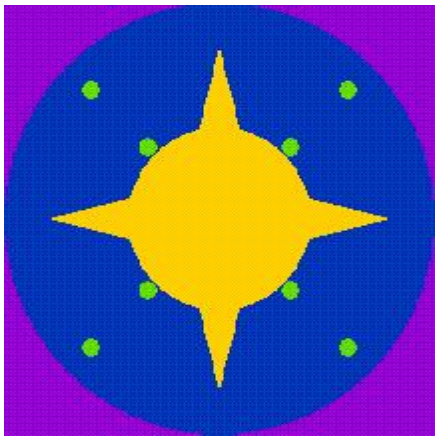

Min = 0.0000 Max = 0.4160
LAvg = 0.3709 AAvg = 0.2689

(b)

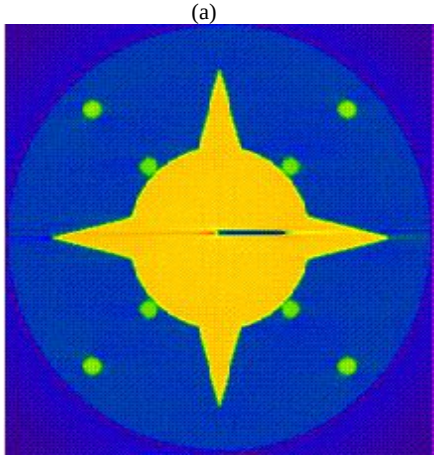

Min = 0.0553 Max = 0.5051
LAvg = 0.3711 AAvg = 0.2700

(c)

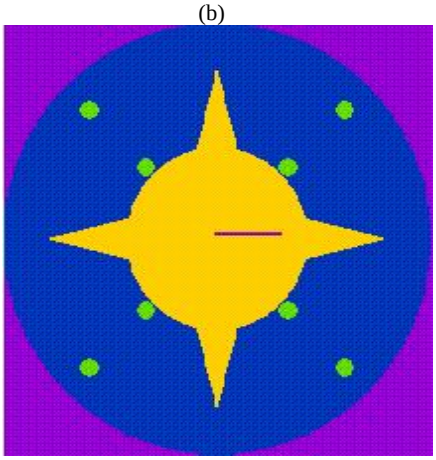

Min = 0.0000 Max = 0.4160
LAvg = 0.3709 AAvg = 0.2681

(d)

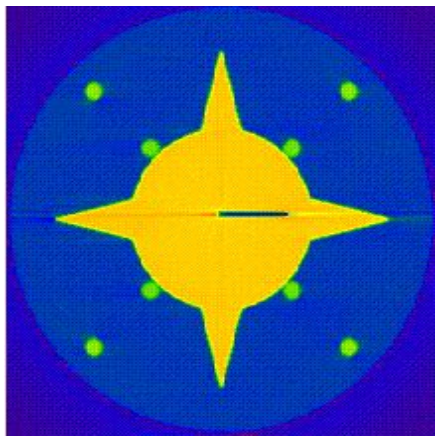

Min = 0.0556 Max = 0.5049
LAvg = 0.3712 AAvg = 0.2700

(e)

Figure 15: Correction for beam hardening on simulated data for star shaped object with a crack for 256 rays and 256 views: (a) Reconstruction of the generated experimental data by directly applying CBP, (b) Simulated object without the crack at energy e_3, (c) Reconstruction after the first iteration of beam hardening correction using fourth degree polynomial at energy e_3, (d) Simulated object with the crack at energy e_3, (e) Reconstruction after the second iteration of beam hardening correction using fourth degree polynomial at energy e_3.

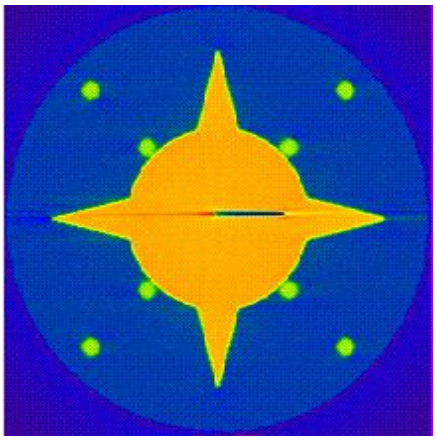

Min = 0.0536 Max = 0.5455
LAvg = 0.3891 AAvg = 0.2812

(a)

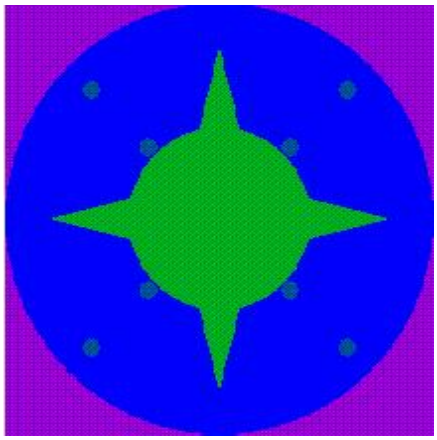

Min = 0.0000 Max = 0.2650
LAvg = 0.2471 AAvg = 0.2065

(b)

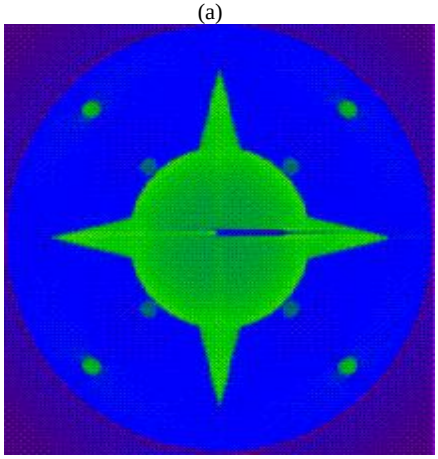

Min = 0.0535 Max = 0.2987
LAvg = 0.2535 AAvg = 0.2071

(c)

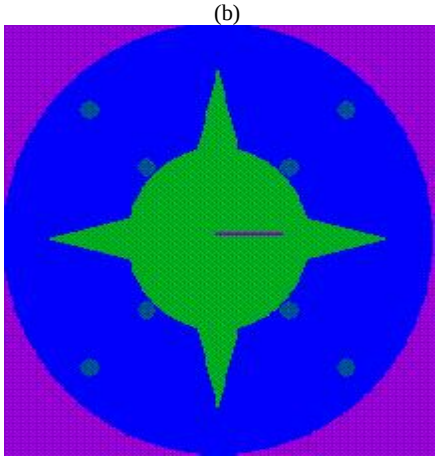

Min = 0.0000 Max = 0.2650
LAvg = 0.2471 AAvg = 0.2060

(d)

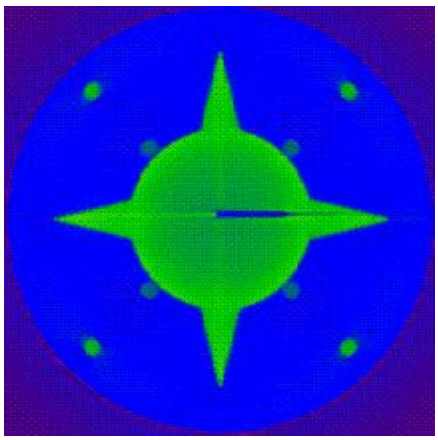

Min = 0.0545 Max = 0.2988
LAvg = 0.2533 AAvg = 0.2077

(e)

Figure 16: Correction for beam hardening on simulated data for star shaped object with a crack for 256 rays and 256 views: (a) Reconstruction of the generated experimental data by directly applying CBP, (b) Simulated object without the crack at energy e_4, (c) Reconstruction after the first iteration of beam hardening correction using fourth degree polynomial at energy e_4, (d) Simulated object with the crack at energy e_4, (e) Reconstruction after the second iteration of beam hardening correction using fourth degree polynomial at energy e_4.

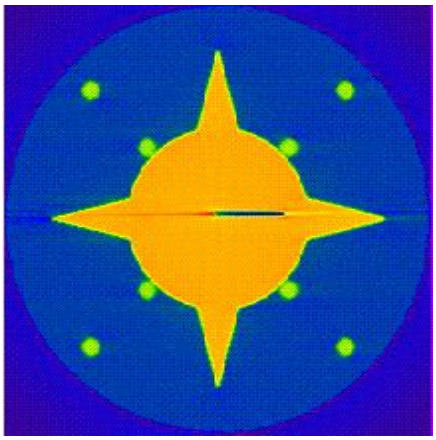

Min = 0.0536 Max = 0.5455
LAvg = 0.3891 AAvg = 0.2812

(a)

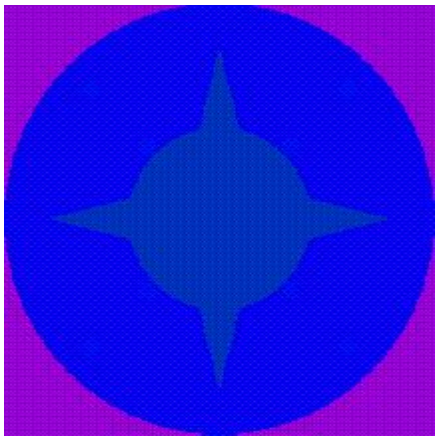

Min = 0.0000 Max = 0.2080
LAvg = 0.2006 AAvg = 0.1837

(b)

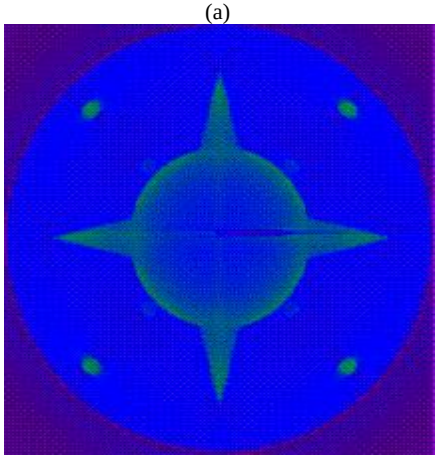

Min = 0.0533 Max = 0.2505
LAvg = 0.2096 AAvg = 0.1852

(c)

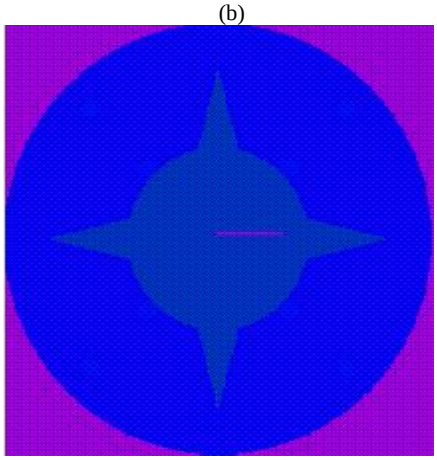

Min = 0.0000 Max = 0.2080
LAvg = 0.2006 AAvg = 0.1833

(d)

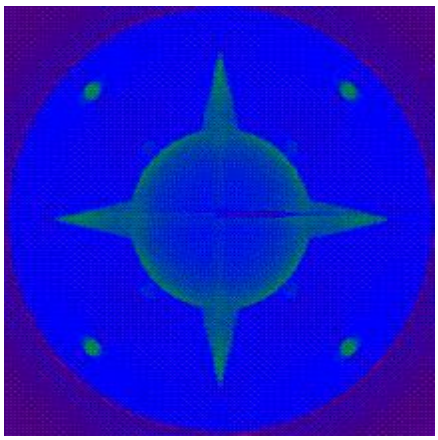

Min = 0.0545 Max = 0.2505
LAvg = 0.2092 AAvg = 0.1850

(e)

Figure 17: Correction for beam hardening on simulated data for star shaped object with a crack for 256 rays and 256 views: (a) Reconstruction of the generated experimental data by directly applying CBP, (b) Simulated object without the crack at energy e_5, (c) Reconstruction after the first iteration of beam hardening correction using fourth degree polynomial at energy e_5, (d) Simulated object with the crack at energy e_5, (e) Reconstruction after the second iteration of beam hardening correction using fourth degree polynomial at energy e_5.